The 2014 ice–jam flood of the Peace-Athabasca Delta: Insights from numerical modelling

Spyros Beltaos

Watershed Hydrology and Ecology Research Division, Canada Centre for Inland Waters, Environment and Climate Change Canada, 867 Lakeshore Rd., Burlington, ON L7S 1A1, Canada

ABSTRACT

Major ice jams forming in the lower reaches of Peace River during the spring breakup of the ice cover are the main agents of flooding and replenishment of the Peace–Athabasca Delta ecosystem. Their paucity following construction of the Bennett Dam (1968) and the potential impacts of climate change have raised concerns regarding habitat degradation. The most recent ice-jam flood, which occurred in 2014, was the fifth in the post-regulation period. Relative to previous occasions, the 2014 event was monitored in considerable detail. Unusually complete water level recordings at Delta hydrometric stations, high-water-mark elevations, and aerial observations furnish adequate quantitative evidence for application of numerical models. Ice-jam modelling capability is essential to quantification of flow magnitudes that help replenish the Delta and can facilitate assessment of climate-change impacts on flood frequency and development of adaptation strategies. Following a brief chronology of the 2014 ice breakup in the lower Peace River and presentation of key hydrometric data, the user-friendly, public-domain model HEC-RAS is briefly described and its setup for the lower Peace River outlined. It is then calibrated and validated on two ice jam configurations that occurred on distinct dates. Application of the calibrated model to different ice-jam scenarios indicated that jams of moderate, rather than extreme, length are more effective in flooding of the Delta.

1. Introduction

The large-river deltas of Northern Canada are unique ecosystems, characterized by some of the highest biological productivity and diversity in the world. The Peace-Athabasca Delta (PAD) in northern Alberta is one of the world's largest inland freshwater deltas, home to large populations of waterfowl, muskrat, beaver, and free-ranging wood bison. The PAD region has been designated a Ramsar wetland of international importance and a UNESCO World Heritage Site. The southern and northern portions of this complex and dynamic ecosystem are periodically re-charged by the Athabasca and Peace Rivers, respectively (Peters and Buttle, 2010). Since the late 1960s, the Peace River sector of the PAD has experienced prolonged dry periods and considerable reduction in the area covered by lakes and ponds that provide habitat for aquatic life. This period coincides with the construction and operation of the W.A.C. Bennett hydroelectric dam in British Columbia, which was completed in 1968, and is located some 1200 km upstream of the PAD. The Peace Canyon dam, located about 25 km downstream of the Bennett dam, was completed in 1980 to enhance generating capacity.

Flow regulation and climatic variability have inhibited the formation of extensive spring ice jams in the lower section of Peace River, which are known to trigger much of the Delta inundation (Prowse and Conly, 1998; Beltaos et al., 2006a). Ice jams cause much higher water levels than open-water floods and are particularly effective in replenishing the higher-elevation, or "perched", basins of the PAD. Concern over the long-term health and sustenance of PAD ecosystems (UNESCO, 2017) is underscored by climate change (Beltaos et al., 2006b) and proposed construction of more dams [the proposed Site C and Dunvegan dams are located some 85 and 275 km downstream of the Peace Canyon dam, respectively; Jasek and Pryse-Phillips (2015)].

In addition to the PAD, post-regulation decreases in ice-jam flood frequency have been documented in China's Yellow River (Chang et al., 2016) and mentioned as a possible factor in the drying of the Saskatchewan River Delta (PFRSB 2009; Abu, 2017); relative contributions by regulation and climate have been delineated by Beltaos (2014) for the PAD and by Chang et al. (2016) for the Yellow River. Since regulation, the PAD experiences major ice-jam flooding about once every 10 years, on the average, as opposed to about once in 5 years prior to regulation (Beltaos, 2014). The 2014 ice-jam flood (IJF for short) was only the fifth since 1968 and the first since 1997. Relative to previous

occurrences, it was documented in considerable detail. The progression of breakup was monitored by various agencies over the entire regulated reach, including the evolving configuration of the final ice jam that caused wide-spread flooding. Unusually complete water level recordings at Delta hydrometric stations provided useful quantitative evidence. Following ice clearance, numerous high water marks were established along the lower 120 km of the river and their geodetic elevations surveyed later in the same year. This information has made it possible to calibrate and apply the HEC-RAS numerical model to the 2014 data and to those of the previous two events (1996 and 1997), for which high water marks are also available. Modelling capability for the lower portion of Peace River is essential to quantification of flow magnitudes that help replenish the Delta and to understanding how jam location and length influence flooding efficacy. Moreover, a reliable model can facilitate assessment of future climate-related impacts on IJF frequency and development of adaptation strategies.

The objectives of this paper are to: (a) present a synthesis of the quantitative information gathered with respect to the 2014 IJF; (b) describe the results of the modelling runs and their implications to the spatial variation of water level and jam thickness; and (c) elucidate how flood levels in the Delta reach of Peace River may depend on the changing length and location of a jam during the evolution of a breakup event.

Following a background section, a brief chronology of the 2014 flood is presented, including relevant hydrometric gauge data and elevations of surveyed high water marks, along with evidence of flow reversals in (normally) tributary channels. The selected numerical model is described next and its setup for the present application outlined. This is followed by the results of the modelling runs, which were extended to include the flood events of 1996 and 1997, as well as scenarios of ice jams of different lengths and locations. Details of hydraulics-based estimates of reverse flow in primary tributaries are also presented.

2. Background information

The Delta reach of the Peace River extends from about Sweetgrass Landing (Fig. 1) to the confluence of Riviere des Rochers (RdR for short), which marks the Mouth of Peace River (MOP) and the beginning of Slave River. Under normal flow conditions, tributary streams like RdR, Revillon Coupe (RC) and Chenal des Quatre Fourches (QF) convey water from Lake Athabasca and other Delta lakes to Peace River (a list of various abbreviations is presented in Appendix A).

When Peace River water levels are high, tributary flow is reduced and may even move in the opposite (reverse) direction under extreme conditions, such as occur during IJFs. At the same time, the normally dry Claire River conveys water to Lake Claire. Aided by concomitant overland flooding, southward flow in tributaries helps recharge the Peace sector of the PAD. The river width typically ranges from 500 to 700 m, but occasionally exceeds 1 km, especially in reaches that contain islands. Bankfull river depth usually ranges from 10 to 15 m, while representative cross-sections can be found in Beltaos (2003). According to Kellerhals et al. (1972) the water surface slope between Peace Point and Carlson Landing is 0.059 m/km; and 0.038 m/km between Carlson Landing and MOP. The latter value is essentially the slope of the Delta reach. Jamming at the Slave River toe location (Fig. 1) is the most common occurrence, likely because jams that initially lodge at upstream sites often re-form in the Slave River after they release. Ice jam length depends partly on the volume of rubble ice that arrives from upstream reaches and typically amounts to tens of kilometers.

A key source of relevant flow and water level data is the hydrometric gauging station at Peace Point (~110 river km above the river mouth; Fig. 1), which has been operated by Water Survey of Canada (WSC) since the late 1950s. Within the Delta reach, the WSC station named "Peace River below Chenal des Quatre Fourches" is located on the southern bank at Rocky Point (Fig. 1) and provides water level data

since 1972. Water levels are also monitored at 3 gauges on RdR. Of these, the northern-most gauge is very close to the MOP and therefore the recorded water levels are also representative of Peace River levels. Useful flow data can also be obtained from the records of the Slave River gauge at Fitzgerald, which is located some 120 km from the MOP.

Table 1 lists the various gauges used herein, along with pertinent details. The end year of the period of record (2nd column) reflects availability of archived data, which are updated periodically; to the writers' knowledge all gauges are active to the present time (July 2018). Data that have been generated but not yet published online could be obtained on request, though they would normally be designated "provisional" and be subject to revision. The distances listed in the last column of Table 1 can vary slightly among different publications, depending on method and map scale used to estimate them. Quoted distances in this paper are consistent with the river chainage presented by Jasek and Pryse-Phillips (2015). For convenience, the two gauges on Riviere des Rochers, are designated RdR-1 and RdR-2, as shown in the first column of Table 1.
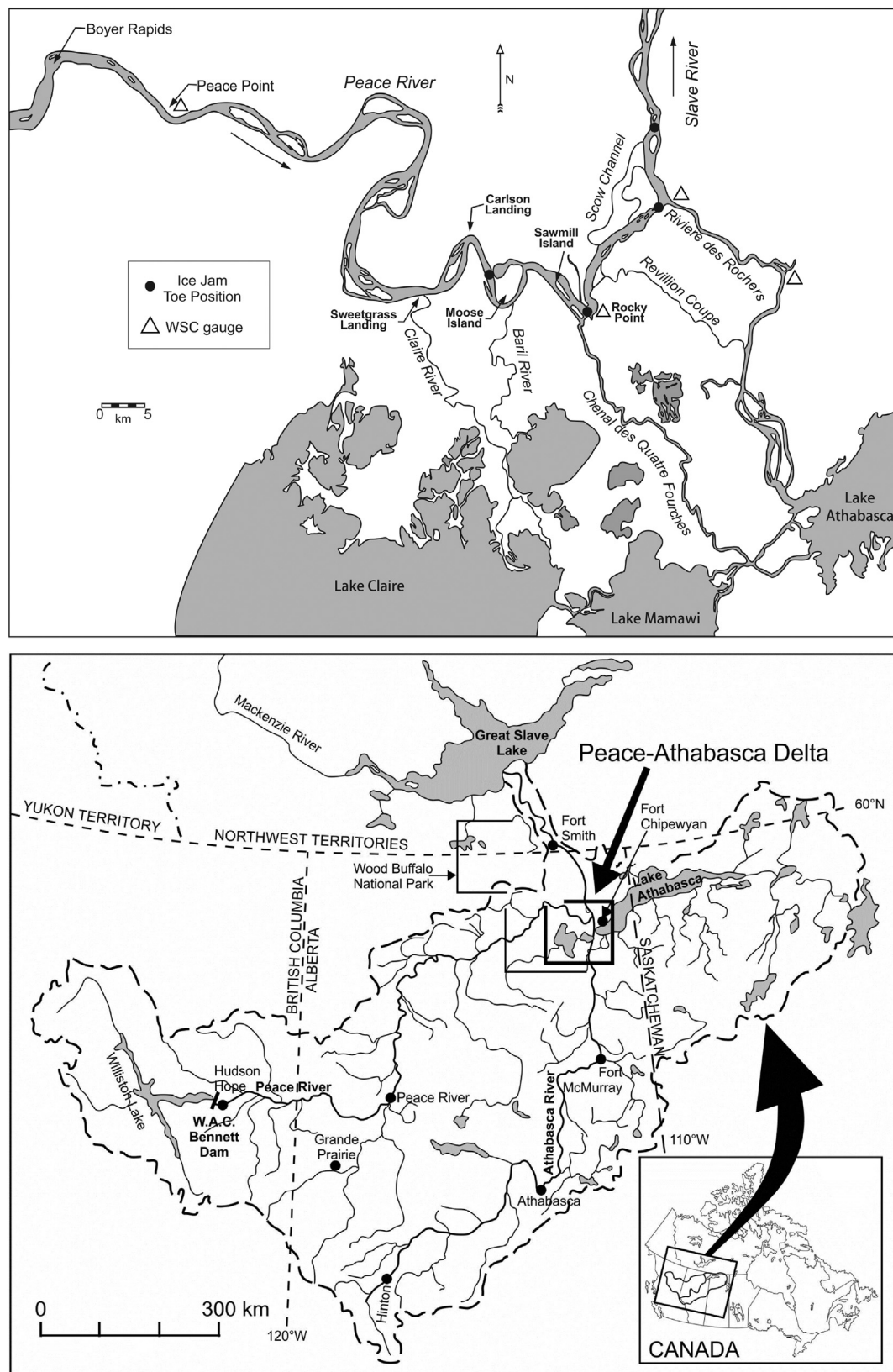
3. The 2014 ice-jam flood event

Comprehensive and amply illustrated chronologies of the 2014 Peace River ice breakup can be found in detailed aerial reconnaissance reports by Straka and Gray (2014) and by Jasek (2017). A brief summary of key events in the last 110 km of the river is presented in this section for convenience. On May 1, an extensive ice run arrived at the mouth of Peace River and was arrested about 10 km into the Slave River, at the usual toe location shown in Fig. 1. The resulting jam grew in the upstream direction as more and more ice rubble arrived at its head (upstream end).

By May 3, the jam extended from the toe in the Slave River to ~7 km downstream of a site known locally as "Burnt Thumb" (Figs. 2 and 3). This 75 km jam was longer than the jam of the 1996 flood but shorter than that of the 1997 flood (Giroux, 1997a, 1997b). Low-lying areas near the major bends above Sweetgrass Landing were flooded. Muddy water from Peace River was evident in Claire River about 11 km south of the Peace. By May 5, the head of the jam had moved a few km downstream and there was some additional flooding, while Peace River water was reaching Lakes Claire and Baril (Fig. 2). By May 6, the jam was showing movement, while the head had moved farther downstream to ~10 km above Sweetgrass Landing (Fig. 2). The extent of flooding had increased, especially to the south of Peace River.

From about May 7 to May 10 there was an ice jam in QF channel, located between 6.5 and 16 km from the confluence with Peace River. The high water levels along this jam caused flow diversions to nearby PAD basins. During May 7 and 8, the head of the Peace River jam continued receding, advancing to below Rocky Point by the 8th of May. The jam released on the 9th and water levels began to recede. Fig. 4 illustrates the overall extent of flooding as observed by Parks Canada (Straka and Gray, 2014). A second QF jam, which was located close to Lake Athabasca is not discussed further herein owing to lack of ancillary data. Fig. 4 also indicates that a short jam formed in RdR above its confluence, likely containing Peace River rubble along with broken-up local ice.

The breakup sequence is reflected in the gauge records of Figs. 5 and 6. From time-lapse images obtained by WSC at Peace Point, it is known that the ice cover was mobilized shortly before 0800 h of May 1 during the passage of a sharp wave (Fig. 5). Farther downstream, the ice cover was very likely mobilized near mid-day, by the waves shown in Fig. 6. Backwater from the lengthening jam in the Slave River would account for the water level rise at Peace Point during May 2 and a portion of May 3; the gradual decline till May 6 (Fig. 5) likely reflects ablation and retreat of the head of the jam. The relatively sharp decrease at Peace Point on May 6 and increase near MOP (Fig. 6) suggest that the upper portion of the jam collapsed and reconsolidated, sending a negative wave upstream and a positive wave downstream. This wave was most

Fig. 1. Plan view of Lower Peace River and Peace-Athabasca Delta. Common ice-jam lodgment sites (or "toes") are shown in the upper portion of the figure. Also shown are sites of Water Survey of Canada hydrometric gauges, of which the records have been used in this study.

likely responsible for the dislodgment of the orifice of the gauge below QF, which is evidenced by the essentially instantaneous drop shown in Fig. 6. The jam collapse would also explain the extensive reduction of

jam length (~33 km) between May 6 and 7; reconnaissance flights on May 7, along with RADARSAT and MODIS images for that day, clearly indicate the head location. After the collapse of May 6, the jam head

Table 1
Water Survey of Canada hydrometric gauge records used in this study.

Station Name	Period of Record	Gauge Number and types of data	Gross drainage area (km^2)	Approx. Location (river km below Bennett dam)
Peace R. at Peace Point	1959–2015	07KC001 Flow/Level	293,000	1135
Peace R. below Chenal des Quatre Fourches	1972–2015	07KC005 Level	No data	1229
Slave R at Fitzgerald	1921–2015	07NB001 Flow/Level	606,000	1360
Riviere des Rochers above Slave River (RdR-1)	1960–2015	07NA001 Level	No data	1243 (0.7)[a]
Riviere des Rochers East of Little rapids (RdR-2)	1960–2016	07NA007 Level	No data	1243 (18)[a]
Lake Athabasca at Fort Chipewyan	1930–2016	07MD001 Level	271,000	NA

[a] For Riviere des Rochers, the distance applies to its confluence with Peace R; gauge distance above the confluence is indicated in brackets.
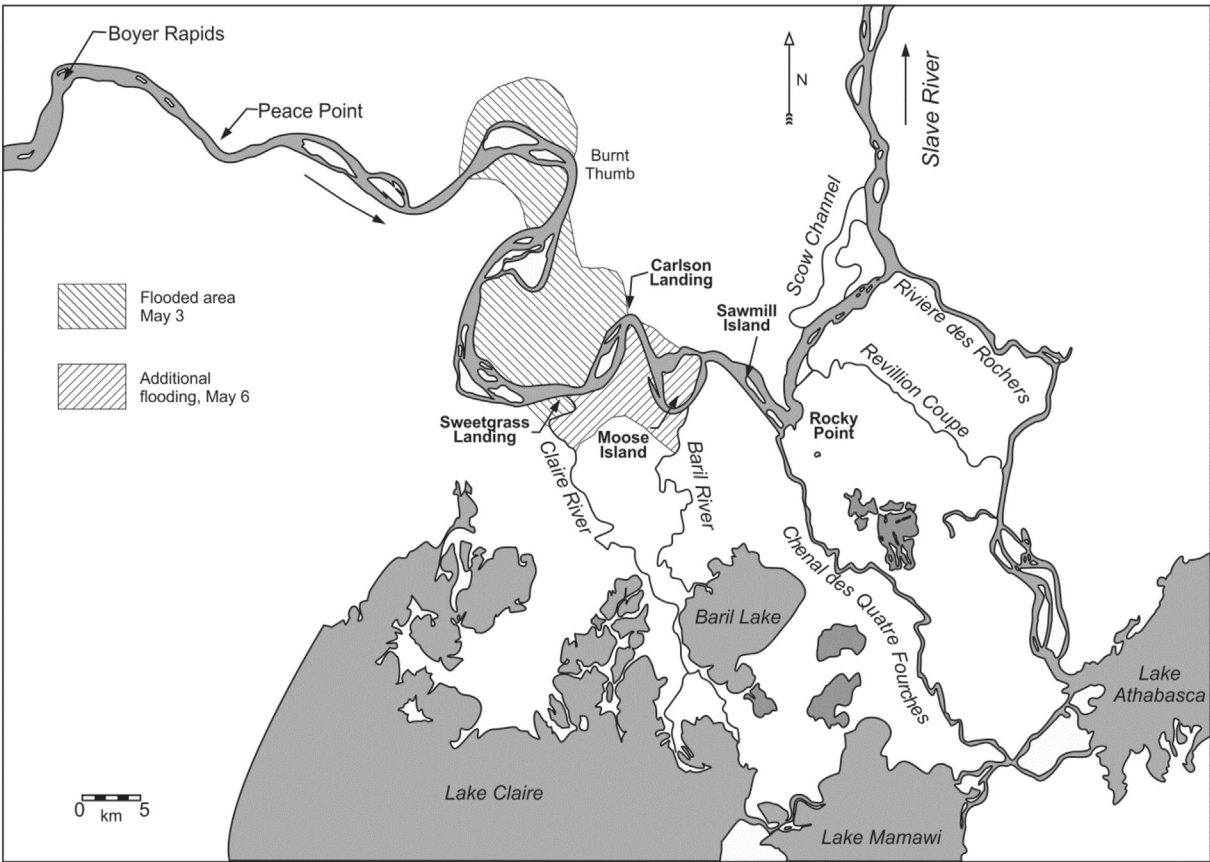
continued to recede through ablation, being several km below Rocky Point (Fig. 1) on May 8. The rapid decrease in water level on May 9 near the MOP (Fig. 7) marks the final release of the jam.

Though not shown in Fig. 4, flow reversal also occurred in RdR, which normally conveys water from Lake Athabasca into the Slave River. This can be inferred from Fig. 7, where the gauge near MOP (marked as "above Slave River") registered higher water level than the gauge farther south during May 1 to 10. Flow reversal in RdR, as well as in RC and QF, was visually evident during aerial reconnaissance on May 3 (Jasek, 2017).

It should be noted here that Water Survey of Canada recently updated gauge-zero elevations of hydrometric stations located in the Lower Peace River (LPR for short), so as to match the Canadian Geodetic Vertical Datum of 2013 (CGVD2013), which was established with the latest GPS surveying methodology. For example, the CGVD1928 elevation of gauge zero at Peace Point (207.121 m) is now reported as 207.246 m. Because the present modelling runs utilize cross sections (XSs for short) that were surveyed prior to 2013 and referenced to the old (1928) datum, it was decided to retain the latter datum throughout this paper. Consequently, all elevations indicated in this paper refer to the 1928 datum.

Shortly after ice clearance from the study area, field crews established high water marks at various locations along the river and within the Delta. These were later surveyed using GPS applications to obtain their elevations and reduce them to the CGVD28 datum. Fig. 8 shows these elevations on a longitudinal profile of the river along with similar data from previous floods. In general, the 2014 flood levels appear to have been intermediate between those of 1996 and 1997.

Fig. 2. Flooded areas along lower Peace River on May 3 and 6, 2014.

Fig. 3. Upstream-looking views of toe (upper) and head (lower) of ice jam on May 3, 2014; note loose accumulation of ice floes near the head. Courtesy of J. Straka and Q. Gray of Parks Canada.

River distances in Fig. 8 were determined in Google Earth using the "path" tool. For the 1996 and 1997 events, these distances are slightly different from, and considered more accurate than, earlier values obtained from 1:50,000 topographic maps (Beltaos, 2003). The same applies to the distances associated with the various cross-sections that have been surveyed to date within the study reach.

4. Selection and set up of numerical ice-jam model

The first application of numerical ice-jam modelling in the LPR was carried out by Demuth et al. (1996) in order to determine flow magnitudes that are needed to cause flooding of the Delta. The public-domain models ICEJAM and RIVJAM were used to calculate water surface profiles along assumed jams of varying length and location, and for different combinations of model parameters. Based on their model runs, Demuth et al. (1996) concluded that a flow of at least 5000 m³/s would be required to cause "macro-scale" flooding of the PAD for jams lodged at Rocky Point or Moose Island (Fig. 1); very long jams, lodged in Slave River near the Scow Channel outfall could cause overbank flooding as far upstream as Claire River with flows as low as 2400 m³/s. The authors pointed out that these results should be viewed with caution owing to several limitations, including sparse bathymetric data and complete lack of model validation data. Shortly after completion of this work, two IJFs occurred (1996 and 1997) and their documentation included surveys of HWMs (Giroux, 1997a, 1997b) while additional bathymetric surveys were carried out in 1999.

With this information, Beltaos (2003) was able to calibrate RIVJAM and determine that a flow of 4000 m³/s would be required at Peace

Point to elevate water levels above portions of the southern river bank in the Delta reach, for assumed jams lodged in the Slave River, at MOP, and at Rocky Point (Fig. 1). Of course, this threshold should be exceeded for a period of a few or several days if significant amounts of water are to be diverted towards the PAD basins. Ice-jam computations could have also been performed with the ice option of the "user-friendly" and also public-domain model HEC-RAS (H-R for short). A major drawback of the latter was, at that time, its inability to interpolate between surveyed XSs. In H-R, computation is carried out between pairs of successive sections that might be several km apart, even though the underlying differential equation requires this length to be infinitesimally small. This deficiency often resulted in unrealistic ice jam profiles (Beltaos et al., 2012). Some years later, a linear interpolation algorithm was added to H-R, rendering its ice routine much more robust. Given also its user-friendliness, and facility with spatially changing flows, this model was selected for the present applications: first to the 2014 jam (May 3 for calibration; May 7 for validation), and then to the less detailed data of the 1996 and 1997 events for further validation.

Both RIVJAM and the ice-jam option of H-R assume steady-flow conditions. This is a reasonable assumption during times when the river flow is changing gradually, e.g. as a result of spring runoff, because temporal gradients in the momentum equation are very small relative to other terms. On the other hand, neither model can capture transient but highly dynamic conditions that typically result from abrupt ice jam releases. Floodplain flow can be modelled with H-R if the applicable topography is known. This is not the case, however, in the present application. Consequently, it is assumed that the flow is confined within the river channel while floodplain abstraction is modelled by a series of sinks, as detailed later. In H-R, the length of the jam is entirely specified by the user while the volume of ice in the jam is a part of the model output.

As noted by Beltaos et al. (2012) and Beltaos and Tang (2013), the distance, L, between successive XSs in the geometry file that is generated by the interpolation "tool" of H-R, affects model output. Too small or too large values of L result in implausible jam profiles, and the user has to exercise some judgment in finding an intermediate range of L values, which produce both stable and plausible profiles. A plausible profile comprises a thickness variation that is consistent with observed and theoretically supported shapes, i.e. characterized by a relatively thick toe, a thin head, and a generally continuous thinning in the upstream direction. If sufficiently long, the jam may also contain a segment of nearly constant thickness ("equilibrium reach"). Profiles that contain unexpected "bulges" in jam thickness and "kinks" in the water level are implausible and typically associated with excessively large spacing of XSs. Such features may also occur when the spacing is too short, which, moreover; leads to jams that are too thin. Output stability can be explored by successively reducing the value of L and comparing the resulting H-R results. Experience suggests that there is a range of L, comparable to the channel width, for which the computed profiles do not change appreciably. For the present applications, L was set at 500 m (channel width ~ 500 to 700 m), prompting the model to generate a geometry file that is based on the surveyed XSs and contains many more synthetic sections that are spaced, as closely as possible, at 500 m intervals.

In addition to bathymetric information, the ice option of H-R requires the following input:

1. River discharge (Q) at the upstream end of the computational reach and at the confluences of significant tributaries or distributaries. This input was guided by WSC flow data at Peace Point and Fitzgerald; and by observed areas of inundation next to the river. Under flood conditions in the LPR, flow is leaving the river channel by spreading over the floodplain or by flowing towards the Delta into channels that are normally tributaries. In the latter case, the under-ice LPR discharge is reduced by an appropriate amount at the
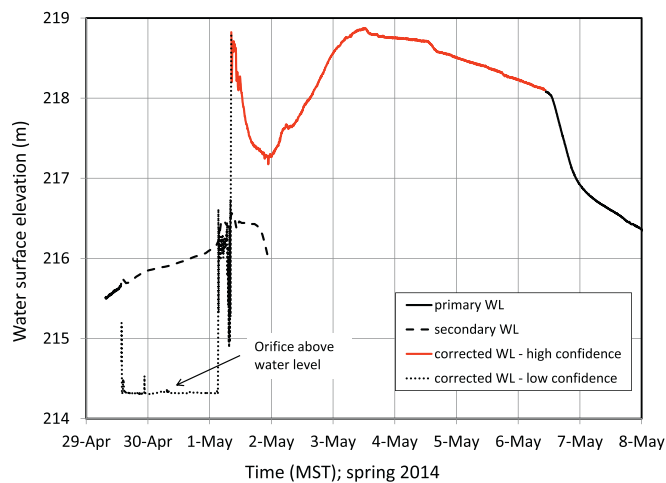
Fig. 4. Maximum extent of May 2014 flooding. Reproduced from Straka and Gray (2014) with permission from Parks Canada.
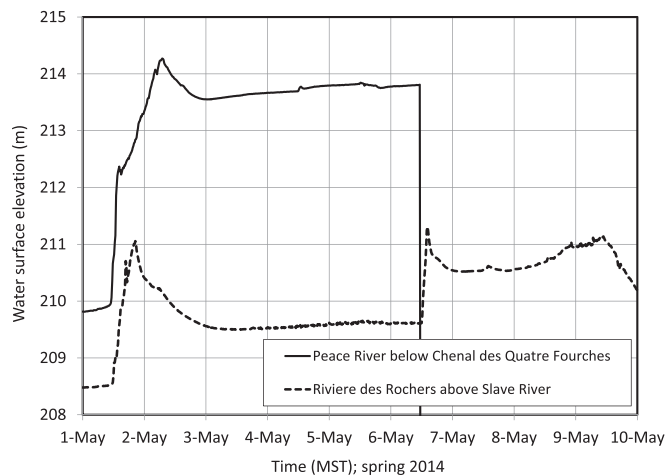
location of the channel mouth. To simulate overland flow, which resembles a distributed sink, a series of closely-spaced point sinks were introduced.

2. Boundary condition at the downstream end of the computational reach, e.g. known water level or normal flow depth. The downstream water level is not known; therefore the latter option was used. It requires the user to specify the local water surface slope, which is also unknown but was assumed to be equal to the known value over the last 35 km of Peace River (0.038 m/km; Kellerhals et al., 1972). According to the H-R manual, the downstream boundary condition suffices where the flow is subcritical, which is typically the case, especially when ice jams are present.

3. Any observed water levels that may be available within the computational reach, to be used in graphical illustrations of calibration runs (optional).

4. Locations of toe (downstream end) and head (upstream end) of the jam. In H-R, river distance is measured in the upstream direction. Because ice jams often extend well into the Slave River, the origin of distance was arbitrarily set at 20 km downstream of the MOP. The toe and head locations were assigned appropriate distances, according to what was observed by aerial reconnaissance (Straka and Gray, 2014).

5. Upstream and downstream limits of open-water and sheet-ice cover reaches. Herein, the sheet-ice cover extended from 0 to 9.5 km,

Fig. 5. Hydrometric gauge record at Peace Point during the 2014 ice breakup. Ice moved the primary orifice line on April 29 but the record was partially corrected by WSC ("high-confidence" line) by applying a constant offset after 0825 h of May 1; the "low-confidence" line is of unknown veracity but helpful as to the pattern of the water level variation. The secondary line is not reliable after about 0300 h of May 1.

Fig. 6. Hydrometric gauge records in the Delta reach (near Chenal des Quatre Fourches) and near the mouth of Peace River (Riviere des Rochers above Slave River).

while open-water prevailed upstream of the jam head.

6. Manning coefficients of river bed and sheet-ice cover (n_b, n_i). Both coefficients were set equal to 0.024, based on detailed slope-area data and analysis for the ice-cover season at the Peace Point gauge (Beltaos, 2011). The value of n_b was corroborated for the entire reach between Peace Point and MOP via open-water H-R runs for June 28, 2011 and Sept. 22, 2016 (Q at Peace Point = 4530 and 2060 m³/s). These runs indicated n_b = 0.023 and 0.024, respectively, based on predicting water levels at the Peace Point and below-QF gauges, starting with concurrent levels at RdR-1 (Table 1).

7. Manning coefficient, n_J, of the underside of an ice jam. This can be a single user-specified value, applicable to the entire length of the jam (default option), or a model-generated function of jam thickness. The latter option (see Appendix B for details) is used exclusively herein, based on past applications that indicated improved model performance (Tang and Beltaos, 2008; Beltaos et al., 2012) as well as on extensive empirical evidence (Nezhikhovskiy, 1964; Beltaos, 2001; Carson et al., 2011).

8. Thickness of sheet-ice cover (t_i). A flow measurement near the

Peace Point gauge by WSC on April 8, 2014 included thickness values at 22 drill holes, spaced at nearly equal distances across the channel width. The average thickness was 0.92 m (max = 1.10 m, min = 0.76 m). Thickness on May 3 has been estimated as 0.80 m, based on the historical pattern of pre-breakup thinning at this site (Beltaos, 2011). This value was applied throughout the computational reach; spatial thickness fluctuations are not expected to significantly affect flow hydraulics, as they are minuscule compared to flow depths.

9. Porosity (p) of the rubble comprising the jam; typically taken as 0.40.

10. Internal friction angle (φ) of the rubble comprising the jam; default = 45° but recent applications indicate considerably higher values (Beltaos et al., 2012; Beltaos and Burrell, 2015).

11. Ratio (K_1) of lateral-to-longitudinal internal stresses within the rubble mass; default value = 0.33. The user's manual offers no other guidance on how to select K_1; consequently the default value has been used in all runs described herein (Appendix B indicates that this choice is physically sound).

12. Maximum allowable flow velocity underneath the jam (V_{max}); default value = 1.5 m/s. Under conditions of high flow the default value may lead to unrealistic results, while a large value that ensures non-exceedance provides an effective practical remedy (rationale is elaborated in Beltaos and Tang, 2013). This may result in unrealistic velocities along a very short river segment at the toe of the jam but produces much more realistic profiles farther upstream (see also Appendix B). A value of 10 m/s was selected for the present runs.

Normally, the computational reach is defined by the first and last surveyed XSs, which in the present case are located at kms 0 and 132. To explore how far upstream backwater effects can persist in a flat river like the Lower Peace when jams are present, a fictional XS was added at km 282. This section was assumed to be identical to that at km 132 but elevated by an amount dictated by the river slope in the vicinity of Peace Point (0.064 m/km).

5. Model runs – 2014 event

5.1. Hydraulic conditions

Inspection of the available gauge records (Figs. 5-7) indicates that peak water levels did not occur simultaneously at different parts of the study reach. At Peace Point, the water level peaked on May 3 as the jam attained its maximum upstream extent (Fig. 5). Further downstream (gauge below QF), the peak occurred on May 2 under fully jammed conditions and the water level remained high on subsequent days, consistent with the continuing presence of the jam. A second peak may have occurred on May 6 during a consolidating ice movement, which appears to have dislocated the orifice line. At the MOP (Fig. 6, RdR gauge), the water level peaked thrice. The first peak occurred late on May 1 due to the developing jam; the water level decreased afterwards, most likely because inflow from this tributary ceased and Peace River water was diverted southward instead. The second peak occurred on May 6 and likely resulted from a consolidating ice movement in Peace River, as described earlier. The water level then decreased slightly, remaining relatively steady during May 7, but gradually increasing afterwards until a third peak on May 9 was followed by final release of the jam. It was therefore decided to apply H-R to two relatively steady-state conditions: one on May 3 with the jam head being at or near its upstream-most location; and May 7, after the consolidating ice movement and reduction of the length of the jam.

The spatial variation of discharge was determined by starting with the Slave River reach. Here, the flow was set equal to next day's flow at the Fitzgerald gauge (Table 1). [Travel time depends on flow magnitude and condition. For ice-covered flow in early May 2014, the travel time
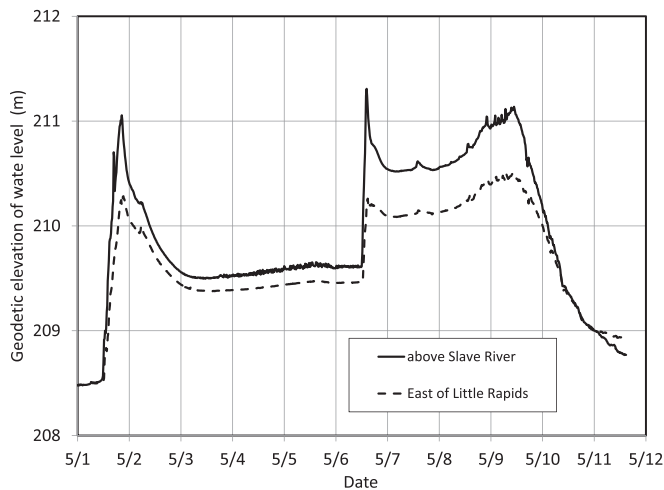
Fig. 7. Riviere des Rochers gauge records (WSC data) in early May 2014. Normally, the flow direction is towards the Slave River and the gauge "East of Little Rapids" registers a higher water level than does the gauge "above Slave River".
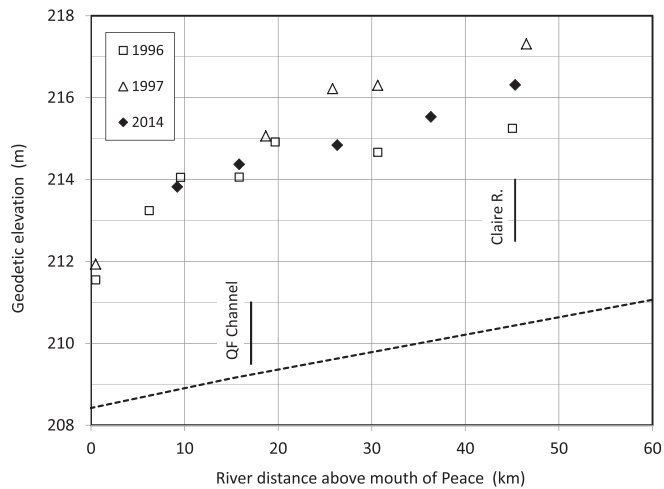

Fig. 8. High water marks along Delta reach of Peace River. The dashed line approximates the water surface profile during May 12 to 14, 2014 (open-water condition; jam released on May 9). "QF channel" is short for Chenal des Quatre Fourches. The 1996 and 1997 data are from Giroux (1997a, 1997b).

between the MOP and the Fitzgerald gauge works out to be 1.3 days for an estimated mean flow velocity of 0.7 m/s and assumed flow-advance rate equal to 1.5 times the velocity (Henderson, 1966)].At the RdR, RC, and QF confluences, independently estimated reversal flows (Section 8) were added consecutively. The resulting flow was then compared to incoming flow at Peace Point on the same, or the previous day, depending on the location of the head of the jam. A significant difference between these two flow values would indicate that flow was either escaping onto the intervening floodplain, or returning to the river from previously flooded areas. A small difference could simply be the result in estimation errors associated with published WSC data and reverse flows in the tributary channels.

5.2. Model run for May 3

The main objective of this run was to calibrate the model by simulating measured water levels at the 3 gauges within the study reach (Peace Point, below QF, and RdR-1; Table 1). According to observations, the toe was at 9.5 km and the head at 85 km but trial runs indicated that the upper 20 km of the jam likely comprised a surface accumulation of ice blocks rather than a thickened agglomerate of randomly oriented blocks that is typical of ice jams (assumed thickness and Manning coefficient of the surface layer = 0.80 m and 0.03, respectively). Had the latter type of accumulation extended all the way to 85 km, the computed water levels upstream of the jam would have been far too high relative to what was indicated by the HWMs and the Peace Point gauge. This assumption is supported by the appearance of the jam near its head on May 3 (Fig. 3, lower photo). At the same time, computed under-ice flow velocities are not large enough to submerge floating blocks, rendering further support to the postulated surface-layer configuration (see Appendix C for details).

River flow at the upstream boundary was taken as 6450 m^3/s, equal to the published WSC Peace Point value for May 3. No travel-time adjustment was made as the head of the jam was located less than a day's travel from the gauge. Between kms 100 and 55, the flow was reduced by equal amounts at 5 km intervals so as to emulate distributed flood-plain loss along the length of the flooded area shown in Fig. 2 for May 3. Reversal flows of 800, 200, and 1000 m^3/s were estimated for QF, RC and RdR, respectively, as detailed in Section 8. The resulting flow variation along the river is summarized in Table 2.

Satisfactory results were obtained with φ = 56°, a value that is consistent with recent simulations (Beltaos et al., 2012; Beltaos and Burrell, 2015). Fig. 9 shows very good agreement between model results and gauge data. There is also general agreement with HWMs upstream of km 40, suggesting that water levels peaked in this reach on
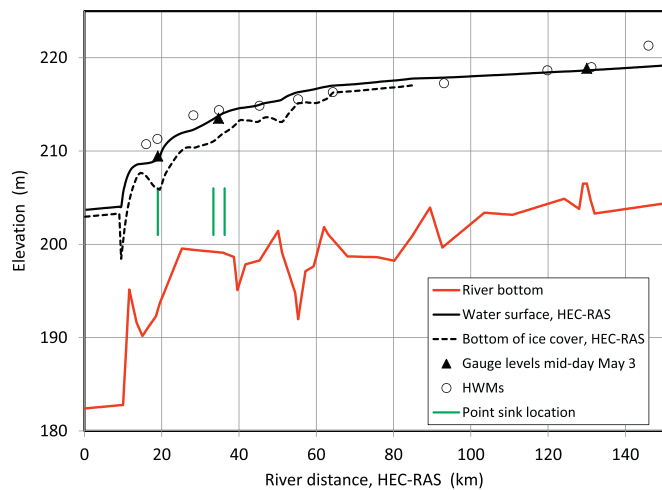
Table 2
Longitudinal variation of river flow used in H-R to account for floodplain inundation and reversal of tributaries.

River km	Flow on May 3, 2014	Flow on May 7, 2014	Flow on April 27, 1996	Flow on April 29, 1997
282	6450	5520	4985	8020
126	6450	5520	4985	Head of jam
100	6450	5520	4985	8020
85	Head of jam			
55	4600	5520	4500	5130
49	4600	5520	Head of jam	5130
43.5	4600	Head of jam	4500	5130
36.3	3800	4520	4200	4500
33.4	3600	4220	4000	4000
19	2600	2920	3260	3400
			(toe at 19 km)	
9.5	2600	2920	3260	3400
	(toe at 9.5 km)	(toe at 9.5 km)		(toe at 10 km)
Fitzgerald gauge, one day later	2600	2920	3260	3160

Fig. 9. Comparing measured water levels to model-generated results for May 3, 2014. Point sinks are mouths of tributaries carrying reversed flow (RdR, QF, RC). The upstream end of the dashed line denotes the head of the jam.
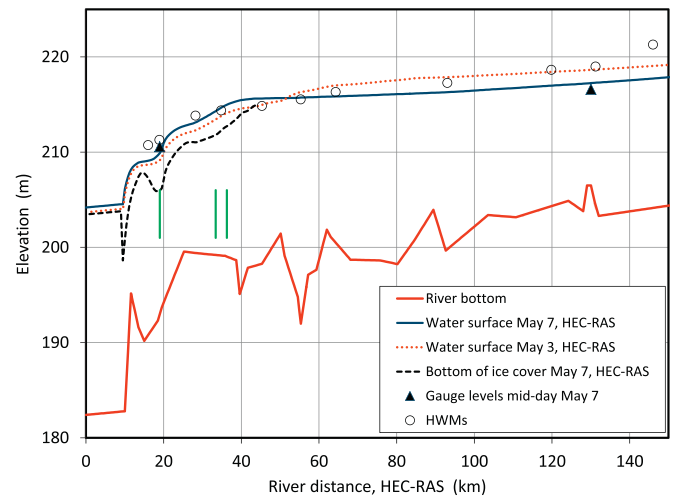

Fig. 10. Comparing measured water levels to model-generated results for May 7, 2014. The lack of a data point for ~km 35, i.e. the gauge below QF, is due to its becoming inoperative upon the May 6 collapse of the jam.

May 3. On the other hand, the HWM at km 146 is about 2 m higher than the model prediction and does not match other HWMs nearby. It was likely attained during brief jamming above Peace Point on May 1, which would have produced the sharp wave shown in Fig. 5 upon release. Downstream of km 35, the computed water levels are below the surveyed HWMs, suggesting that the latter were attained at a different time, possibly during the jam collapse of May 6 (Fig. 6).

Typical jam thickness values in Fig. 9 range from 2 to 3 m. They are comparable to values computed by RIVJAM for the 1996 and 1997 jams (Beltaos, 2003); and to visually estimated shear wall heights that formed after the release of an ice jam in 2007 (Beltaos and Carter, 2009). The conspicuous "bump" in jam thickness at ~km 20, which is also present in subsequent model runs, is caused by: (a) the diversion of a sizeable amount of flow into RdR and towards Lake Athabasca; and (b) the local river morphology, where the relatively narrow channel above RdR merges into the much wider Slave River (Fig. 1). Trial runs with and without the RdR "sink" showed that the bump is less pronounced when the sink is removed. A model run for a hypothetical prismatic channel also indicated bump formation in the vicinity of a flow sink.

5.3. Model run for May 7

As noted earlier, the length of the jam decreased gradually after May 3 and abruptly on May 6, likely as a result of collapse and re-consolidation. The nearly steady-state condition that prevailed near the MOP during May 7 (Figs. 6 and 7) offers an opportunity to validate the calibrated model. The toe of the jam remained unchanged but the head was now at km 43.5. To determine the spatial variation of discharge, the May 8 flow at the Fitzgerald gauge was adopted as the flow downstream of the MOP, while estimated outflows (Section 8) at the three lower tributary mouths were taken into account, to find a discharge of 5520 m^3/s upstream of QF (Table 2). Comparison of this figure with flow at Peace Point a day earlier (5560 m^3/s) indicated that there was essentially no flow change upstream of QF. This finding also implies that the May 3 flow diversion to the northern floodplain (Fig. 2) had ceased by May 7.

Using the flows indicated in Table 2, H-R was applied to the May 7 jam with the same parameters as for May 3 and the results are shown in Fig. 10. One may note that the computed May 7 water level profile matches the gauge reading below QF but does not adequately reproduce the two lower HWMs; this reflects the fact that the latter were likely attained during the jam collapse on May 6. Fig. 6 shows that the peak water level near the MOP RdR above Slave River was ~0.7 m

higher than the steady-state level of May 7 and very nearly accounts for the local difference between modelled profile and HWM. The ~2 m discrepancy at km 16, however, is difficult to fully explain at present. It can be concluded that the HWMs in the lower reach represent brief peaks of dynamic nature, while the computed, slightly lower, water levels were more sustained and thence more effective in terms of flooding.

The increase over the May 3 flows downstream of km 55 (Table 2), despite lower incoming flow at Peace Point, can be attributed to the downstream movement of the jam head and accompanying decrease of water levels in the now open reach. This decrease would have ended local flooding and allowed more river water to reach the jam.

6. Effect of jam length and location

The 2014 IJF event began with a very long jam, extending as far upstream as Burnt Thumb. Observations and modelling runs indicated that this configuration is associated with floodplain inundation along the segment ~55 to ~100 km, occurring mostly on the left (facing downstream) side of the river. Consequently, the flow arriving to the
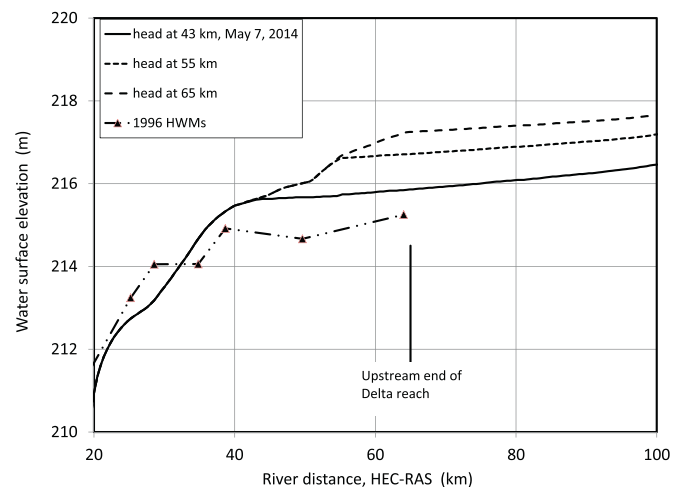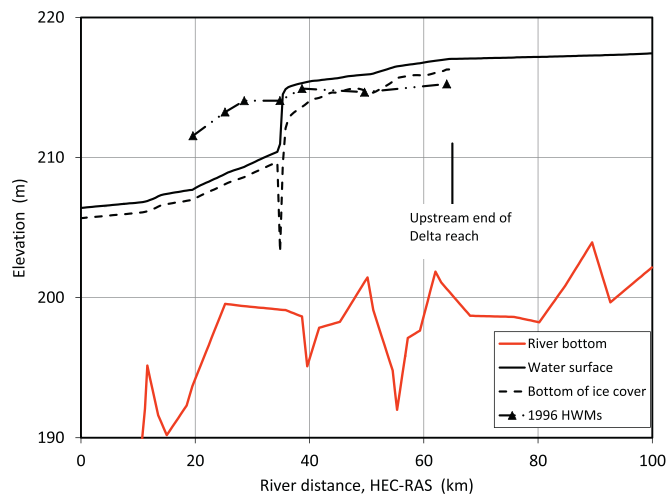

Fig. 11. Water level profiles computed by H-R for different jam lengths with the flow conditions prevailing on May 7, 2014. High Water Marks from the 1996 IJF, which was lesser than the 1997 event but did result in considerable replenishment of the perched basins (Peters et al., 2006), are also plotted for comparison.

Fig. 12. Modelled profile of a jam lodged at Rocky Point with the flow conditions approximating those of April 28, 1994 (Peace River flow ~ 5300 m³/s; Slave River flow = 4600 m³/s); the unknown jam head location was set at 65 km.

Fig. 13. Comparing measured water levels to model-generated results for April 27, 1996. No data point available for Peace Point gauge (km 130).

Fig. 14. Comparing measured water levels to model-generated results for April 29, 1997.

lower portion of the jam is considerably less than the Peace Point value (Table 2: May 3, 2014 and April 29, 1997).
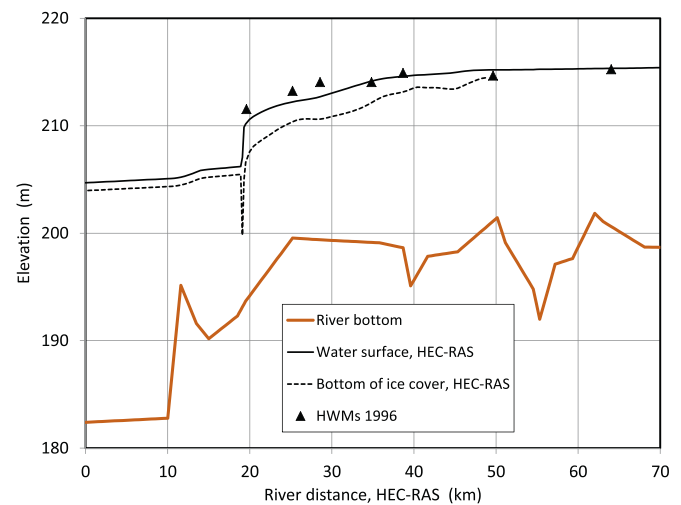
When the long jam collapses and shortens, the flow under it increases because water levels farther upstream decrease while lateral escape onto the floodplain is reduced and possibly even reversed. For instance, Table 2 shows that the May 7 flow is higher than the May 3 flow within the Delta reach. This configuration is ecologically desirable because larger amounts of water are now directed southward into the Delta basins. Over time, the head of the shortened jam recedes as a result of ablation and this effect gradually diminishes the spatial extent of flooding, until the jam finally releases.

Using the calibrated model, it is possible to explore how the jam length influences the water level profile when the jam toe is located in the Slave River (as in 2014) while the head is within the Delta reach. Fig. 11 shows that water levels would have been significantly higher in the upper 20 km of the Delta reach if the May 7 jam had been longer. The spatial variation of the flow was assumed for simplicity to be the same as the one shown for May 7 in Table 2, but the higher water levels upstream of the longer jams might have diverted some flow onto the floodplain, thus reducing the flow underneath the jam. This effect is difficult to quantify. It can nevertheless be concluded that the ecologically optimal configuration of a jam occurs when the head is located near km 65 and the toe ~10 km into the Slave River. Jams with toe locations within the Peace River itself are less effective, as is shown next.
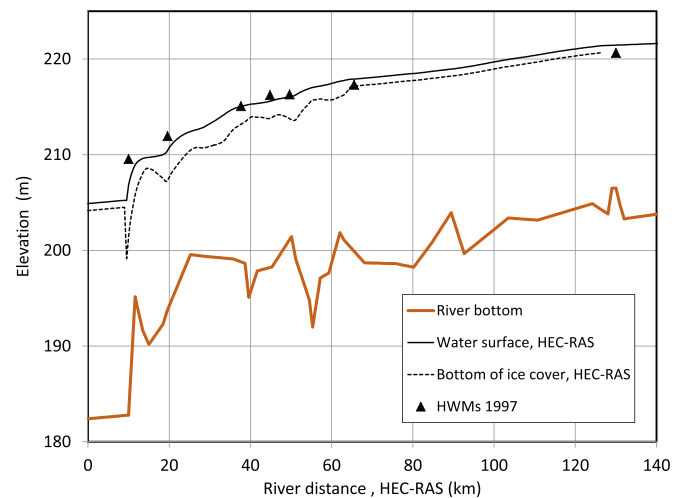
Apart from the Slave River lodging site, ice jams are known to lodge at other Peace River locations, such as Rocky Point (Fig. 1). It is known for instance, that a jam formed at this site on April 28–29, 1994, causing "moderate" flooding (Timoney, 2009). Assuming the unknown head location of this jam to have been at 65 km (~upstream end of the Delta reach), the calibrated H-R generated the profile shown in Fig. 12. Though water levels upstream of the jam are high, its limited length suggests that any associated flooding of the PAD would have also been limited, as was actually the case.

7. Model runs - 1996 and 1997 events

As noted earlier, Beltaos (2003) applied the model RIVJAM to two sets of HWMs that were surveyed after each event (Giroux, 1997a, 1997b). No gauge data were available for the Delta reach because the LPR and RdR gauges were rendered inoperative by ice. Therefore, reverse flows in the three lower tributaries were selected so as to optimize

model output while guided by unpublished results of the ONE-D model (Beltaos, 2003).

Though the 1997 jam extended to ~km 126, the RIVJAM computation was terminated at km 63 as there were no river XSs at that time between this location and the vicinity of Peace Point. Later surveys have furnished additional XSs, enabling application of H-R runs to Peace Point and beyond. The beginning for the surface-type accumulation was taken as 65 km, as was found for the long jam of May 3, 2014.

To examine how the calibrated model performs in the case of the 1996 and 1997 events, the internal friction angle was again set at 56° while the spatial variation of the flow within the jammed reach was taken to be the same as that which was used in RIVJAM (Beltaos, 2003). Model predictions are compared to respective sets of HWMs in Figs. 13 and 14. Agreement is generally good above km 30 but the predicted water levels are on the low side below km 30. This could reflect non-simultaneity of the HWMs and/or occurrence of highly transient peaks, as was the case in 2014 within the same segment of Peace River. Over-prediction of the water level at ~km 50 in Fig. 13 and ~kms 65 and 130 in Fig. 14 could reflect HWM identification and survey errors. In the case of Fig. 14, which involves two data points, it is also possible that the surface accumulation of ice blocks in the upper portion of the jam

may have been thinner and smoother, or extended farther downstream, than in 2014.

8. Reverse flow in tributaries

Of particular relevance to the present study are the flow conditions in the three lowermost tributaries, RdR, RC, and QF on May 3 and 7, 2014. Measurements by others (BC Hydro, 2013) during the years 2002 to 2004 have indicated that, under open-water conditions, RdR flow into LPR amounts to 5 to 7 times that of QF and 20 to 30 times that of RC. Flow measurements on Oct. 4, 2017 indicated values of 1223, 49 and 285 m^3/s for RdR, RC and QF, respectively (all flowing into LPR), indicating that RdR carried 4 and 25 times the flows of QF and RC. In terms of the total flow delivered to LPR by these tributaries, the respective percentages were 79, 3, and 18%. Using previously obtained bathymetric measurements in RdR and QF, the measured flow and corresponding slope values indicated respective bed Manning coefficients, n_b, of 0.028 and 0.026. These values are similar to indirect assessments with the model ONE-D and limited bathymetric information (Pietroniro et al. 2011), indicating essentially identical n_b values for QF, RC and RdR (0.024, 0.026, and 0.025, respectively).

Noting that tributary slopes are very small, so that small differences in n_b may simply reflect very small elevation errors, a common value of 0.027 was assumed for both QF and RdR. For simplicity, an equal value was used for n_i, the sheet-ice coefficient of these channels in early May of 2014, taking into account that significant underside roughness develops during the pre-breakup period (Carey, 1966, 1967). The sheet-ice thickness was taken as 0.8 m, same as in Peace River. As noted in Section 3, observations and local water level data pointed to conditions of reverse flow (outflow from LPR) in RdR, RC, and QF during the breakup period.

Outflows for May 3 were calculated by applying the slope-area method and using known water levels at gauges RdR-1, RdR-2, PR below QF, and Lake Athabasca at Fort Chipewyan (Table 1). At this time, these channels were still covered with sheet ice. As there are no water level data for RC, its relatively small flow was "guesstimated", guided by what was calculated for the two larger channels. Resulting errors would, in any case, be very small relative to the Peace River flow.

The QF outflow for May 7 was determined by applying the calibrated H-R model in the jammed reach (Fig. 4), and varying the discharge until good agreement was obtained between computed water level at the mouth of QF and the reading of the Peace River gauge, which is located just a short distance downstream. The resulting water level profile indicated overbank flow, in agreement with observations. A similar application of H-R to the May 7 condition of RdR "failed", in

the sense that the model could not generate a jam that would conform to the measured water levels at RdR-1 and RdR-2. This means that the observed jam was not of the kind assumed in H-R ("wide-channel jam", as first defined by Pariset et al., 1966). Most likely, this jam consisted of rubble from Peace River that was pushed into RdR as the flow reversed, causing limited breaking of the local ice cover. A constant thickness of 2.5 m was assumed for this rubble layer, comparable to modelled values for Peace River in the vicinity of the RdR mouth. Its Manning coefficient was taken as 0.095, consistent with Nezhikhovskiy's (1964) findings for ice-block accumulations. The model was then applied between RdR-1 and RdR-2, assuming sheet-ice cover downstream of the rubble. A flow of 1300 m^3/s was found to adequately reproduce the water level at RdR-1 using the water level at RdR-2 as the downstream boundary condition (see also Fig. 7). Table 3 summarizes the estimated outflows for the model runs in LPR for May 3 and 7. Water surface slope is simply hydraulic head over total channel length between PR and Lake Athabasca.

9. Discussion

The preceding results have quantified the evolution of IJF water levels during the major ice-jamming events of 2014 in the PAD, elucidated the non-simultaneity of HWMs, and characterized the flooding potential of different ice-jam configurations. At the same time, the good performance of the calibrated H-R model renders it a reliable tool for future use in a variety of practical applications. One of these pertains to the release of extra water from the Bennett Dam at opportune times, in order to raise ice-jam water levels in the PAD area. This was done with some success during the 1996 breakup event (Prowse et al., 2002) and could be considered in the future as an adaptive strategy to alleviate expected adverse climate-change effects (Beltaos et al., 2006b). For instance, it would be of interest to quantify the magnitude and duration of an effective flow release using H-R for a range of anticipated spring flows and for a few scenarios of ice jam location and persistence. This kind of information would be helpful in planning release operations in years when fall and winter hydroclimatic conditions are favourable to formation of a major spring ice jam in the PAD (Beltaos et al., 2006a).

As noted in Section 2, re-charge of the PAD, and especially of the perched basins, depends on overland flooding and tributary reversals. Reverse flows in QF and RdR also help replenish L. Athabasca which largely controls the levels of smaller Delta lakes and ponds during normal (non-jam) conditions. It is only with ice-jam modelling, such as H-R, that the magnitudes of reverse spring breakup flows can be quantified. Because PAD ice jamming is the last phase of breakup over several hundred km of Peace River (Beltaos and Carter, 2009), the

Table 3
Estimated reverse flows in lower tributaries on May 3 and 7, 2014.

Date	Parameters	QF	RC	RdR
May 3	Flow (m^3/s)	800	200	1000
	Ice conditions	Sheet-ice cover	Sheet-ice cover	Sheet-ice cover
	Method of Flow estimation	Slope-area	~10% of total outflow (assumed)	Slope-area
	Peace River WL at confluence (m)	213.52[2]	unknown	209.51[4]
	Lake Athabasca WL[1] (m)	209.02	209.02	209.02
	Water surface slope (m/km)	0.082	unknown	0.010
May 7	Flow (m^3/s)	1000	300	1300
	Ice condition	Ice jam	Sheet-ice cover	2.1 km rubble accumulation, followed by sheet-ice cover
	Method of Flow estimation	H-R	~10% of total outflow (assumed)	H-R
	Peace River WL at confluence (m)	214.6[3]	unknown	210.55[4]
	Lake Athabasca WL[1] (m)	209.29	209.29	209.29
	Water surface slope (m/km)	0.097	unknown	0.027

[1] WSC gauge at Fort Chipewyan [2] assumed approximately equal to nearby Peace River gauge reading; gauge located 1.5 km below confluence; [3] no gauge data on May 7; water level estimated from nearby HWM; [4] assumed approximately equal to RdR-1 reading; gauge located 0.7 km south of confluence.

modelling reach is likely to be extended in the future. Availability of a calibrated model would then be advantageous. Changing climatic conditions over the Peace River basin are likely to reduce spring breakup flows in the PAD (Beltaos et al., 2006b) via enhanced mid-winter thaws and reduced spring snowpacks. The associated effects on local ice-jam water levels can be quantified using the calibrated H-R for different climate and flow scenarios.

The various model runs indicated that backwater persists for very long distances upstream of the head of an ice jam in Peace River. For the April 29, 1997 occurrence (head at km 126) backwater was still present at the end of the computational reach (km 282). For the April 27, 1996, May 3, 2014, and May 7, 2014 occurrences, backwater persisted for respective distances of 167, 148, and 175 km upstream of the jam head. [Backwater was considered negligible where it caused an increase of 2% or less over the uniform flow depth]. Consequently, the open-water rating relationship for the Peace Point gauge (located 110 km above the MOP) may overestimate the river flow when ice jams are present in the Delta reach, even where the jam head is located tens of kms below the gauge. For instance, the head of the May 7, 2014 jam was located ~87 km downstream of the Peace Point gauge, but the available WSC flow and gauge data suggest a backwater of 1.3 m. The corresponding difference in flow is ~2500 m^3/s.

The volume of ice that was available for transport to the Delta before the ice run of April 30 and May 1, 2014 is estimated as 180 million m^3 (180 Mm^3) based on known initial ice conditions and assuming average sheet-ice thickness and river width of 0.8 m and 600 m, respectively. On May 3 and 7, the volume of ice in the 75 and 33 km jams has been estimated by H-R as 81 and 52 Mm^3, respectively. The volume reduction (99 Mm^3) between April 30 and May 3 is due to melt as well as stranding of ice floes in shallow areas near river banks and islands. Stranding was likely the dominant attrition factor, given the long reach (over 300 km) of ice cover that was cleared during April 30 and May 1. On the other hand, the volume reduction of 29 Mm^3 between May 3 and 7, would have been primarily caused by melt. Neglecting the volume of any stranded ice, results in a melt rate of ~7 Mm^3/day. For a jam on the Liard River, Prowse (1986) reported a total (ice and water) reduction in ice jam volume of 6.7×10^5 m^3/h. As the estimated jam porosity was 0.38, the daily rate of melt is calculated as $6.7 \times 10^5 \times 24$ x $(1–0.38) = 10.0$ Mm^3/day. Of course, such rates can vary with incoming discharge and water temperature but the preceding estimates indicate similar magnitudes in these large northern rivers of comparable width.

The data of Table 3 suggest that RdR remains the primary channel during conditions of flow reversal, but QF now conveys a comparable discharge (~80% of RdR flow), as opposed to a near-order of magnitude difference (14% to 20%) under normal open-water conditions. This can be explained by the relationship between respective hydraulic heads between Peace River and Lake Athabasca. In normal mode, the surface of Lake Athabasca is at a higher elevation than the lower portion of Peace River. Consequently the hydraulic head of RdR exceeds that of QF because the mouth of QF is located upstream of the mouth of

RdR. Coupled with the larger cross-sectional area of RdR, this effect explains the large difference between RdR and QF flows under normal conditions. In reversal mode, the Lower Peace water levels exceed the elevation of Lake Athabasca and therefore the hydraulic head of QF exceeds that of RdR; and such excess is exacerbated by the presence of an ice jam in Peace River. This effect partly offsets that of channel cross-sectional area and renders QF flow comparable to RdR flow.

10. Summary and conclusions

The 2014 IJF of the PAD supplied much needed replenishment to Delta ecosystems after a 17 year hiatus. It resulted from the release of two jams downstream of Fort Vermilion and subsequent ice mobilization and breakup in the last 300 km of Peace River on April 30 and May 1, 2014. The ice run was arrested about 10 km into Slave River, a known lodgment site. With the continuous arrival of rubble, the jam increased in length until May 3, and then gradually shortened by ablation. Its upper portion collapsed on May 6, and the resulting shorter jam remained in place until May 9.

The relatively complete data set of 2014 has been used for calibration and validation of the ice routine of the user-friendly, public-domain, model HEC-RAS. The model was calibrated using the jam conditions of May 3 and validated with the conditions of May 7 using the following options and parameters: XS interpolation distance = 500 m; ice jam Manning coefficient = variable; V$_{max}$ = 10 m/s; K$_1$ = 0.33; internal friction angle φ = 56˚.

A unique feature of the 2014 documentation is the evidence regarding non-simultaneity of the surveyed HWMs, which enabled more insightful modelling applications than had been possible in the case of the 1996 and 1997 events. The 2014 ice-jam model runs indicated that wide-spread flooding of the Delta occurred after the initially very long jam collapsed and shortened, so as to be located entirely within the Delta reach. Exploratory test runs showed further that the optimal jam configuration for re-charging the PAD extends from the Slave River to, or somewhat downstream of, km 65.

Reverse flow in the ice-covered tributary channels QF and RdR was estimated using measured hydraulic heads and surveyed cross sections for the conditions prevailing on May 3, 2014 (sheet ice cover) and May 7, 2014 (ice jam). These estimates suggest that, unlike open-water, forward-flow conditions, QF carries comparable reverse flow to that of RdR when an ice jam is present in LPR.

Appendix A. List of abbreviations

H-R	HEC-RAS
HWM	High Water Mark
IJF	Ice-Jam Flood
LPR	Lower Peace River
PAD	Peace-Athabasca Delta
QF	Chenal des Quatre Fourches
RC	Revillon Coupe
RdR	Riviere des Rochers
RdR-1	RdR gauge above Slave River
RdR-2	RdR gauge East of Little Rapids
XS	Cross section
WSC	Water Survey of Canada

Appendix B. background information on the physics and practical use of the HEC-RAS model

B.1. Variable ice-jam roughness

The Manning coefficient of the underside of an ice jam (n_J) is known to depend primarily on ice jam thickness and secondarily on flow depth (Nezhikhovskiy, 1964; Beltaos, 2001). Under the variable-roughness option of HEC-RAS, n_J is estimated as follows (English units):

$$n_J = 0.069H^{-0.23}t_J{}^{0.40} \quad for\ t_J\ >\ 1.5\ ft \tag{B1}$$

$$n_J = 0.059H^{-0.23}t_J{}^{0.77} \quad for\ t_J \leq 1.5\ ft \tag{B2}$$

in which t_J = ice jam thickness in feet; and H = total water depth in feet (HEC-RAS, 2010). It can be shown that the numerical coefficients in Eqs B1 and B2 would change to 0.084 and 0.113, respectively, when metric units are used.

B.2. Model coefficient K_1

As noted in Section 4, the H-R manual suggests a default value of 0.33 but gives no guidance as to how K_1 may change under different modelling conditions. This coefficient derives from early ice-jam theory (Pariset et al., 1966), which is the basis of the H-R ice jam routine. According to this theory, which implicitly assumes that the least and intermediate principal stresses within the jam are equal, K_1 is given by (Flato and Gerard, 1986):

$$K_1 = \frac{1 - \sin^2\varphi}{1 + \sin^2\varphi} \qquad (early\ theory) \tag{B3}$$

According to Eq. B3, the K_1 value of 0.33 corresponds to the default internal friction angle of 45°. For $\varphi = 56°$ (value selected in the present calibration), Eq. B3 results in $K_1 = 0.19$. However, Beltaos (2010) has shown that the early theory is incorrect because the least and intermediate principal stresses within the jam are not equal; instead he adopted the following equation, which derives from the lateral confinement (zero lateral strain) of the rubble within the jam:

$$K_1 = \nu\left(1 + \frac{1}{K_x}\right) \qquad (Beltaos\ 2010) \tag{B4}$$

in which ν = Poisson ratio; and K_x = ratio of longitudinal-to-vertical internal stresses within the jam. For expected values of K_x (~7 to 15), Eq. B4 indicates that K_1 is nearly a constant, averaging 0.33 for $\nu = 0.3$ (commonly used value for granular materials; Serré et al., 2010). Fixing the value of K_1 at 0.33 is therefore physically sound.

B.3. Limiting toe velocity, V_{max}

The physical significance of this parameter is that where V_{max} is exceeded, ice blocks at the bottom of the jam will be mobilized and transported away by the flow (Flato and Gerard, 1986). Ice jams are thickest near their toe, owing to large local water surface slopes (Beltaos and Wong, 1986; Beltaos, 2001). The accompanying reduction in unobstructed flow area can lead to large computed under-ice velocities (V) if flow through the voids of the jam is neglected, as is done in H-R. Where a jam thickens to the extent that V exceeds V_{max}, H-R ignores the jam stability equation and computes the jam profile by setting $V = V_{max}$. It is therefore implicitly assumed that the jam is continuously collapsing within such regions, being prevented from attaining the stability-dictated thickness because it is being eroded by the flow. On the other hand, models that do take into account flow through the voids of the jam (e.g. RIVJAM; Beltaos, 1993, 1999) can satisfy stability criteria throughout the jam length without generating excessive under-ice velocities. With a user-selected very large value of V_{max}, H-R is able to compute more realistic profiles in the toe area of the jam. Resulting violations of the erosion criterion are only apparent because in reality under-jam velocities remain moderate, owing to flow through the jam voids.

Appendix C. Submergence velocity of ice blocks

Ashton (1974) determined the critical under-ice submergence velocity (V_{subm}) of an ice block, as follows:

$$\frac{V_{subm}}{\sqrt{(1 - s_i)gt_i}} = \frac{2}{\sqrt{5 - 3\left(1 - \frac{t_i}{H}\right)^2}} \tag{C1}$$

in which g = acceleration due to gravity; t_i = ice block thickness; and H = total water depth = under-ice depth of flow plus submerged portion of block thickness. For the May 3, 2014 run, V_{subm} is almost constant at 1.02 m/s in the surface-layer reach, while the under-ice velocity does not exceed 0.77 m/s. For the 1997 run, V_{subm} is again nearly constant at 1.02 m/s, while the under-ice velocity is less than this value, with the exception of a short stretch (km 109 to km 114). Here V_{subm} is exceeded, but the excess is very slight (up to 6 cm/s).

References

Abu, R., 2017. Knowledge, Use, and Change in the Saskatchewan River Delta: Assessing the Changing Livelihoods of Cumberland House Métis and Cree Nation. Ph.D. Thesis. School of Environment and Sustainability, University of Saskatchewan, Saskatoon.

Ashton, G.D., 1974. Froude criterion for ice block stability. J. Glaciol. 13 (689), 307–313.

Beltaos, S., 1993. Numerical computation of river ice jams. Can. J. of Civ. Eng. 20 (1), 88–99.

Beltaos, S., 1999. Flow through breakup ice jams. Can. J. of Civ. Eng. 26 (2), 177–185.

Beltaos, S., 2001. Hydraulic roughness of breakup ice jams. ASCE Journal of Hydraulic Engineering 127 (8), 650–656.

Beltaos, S., 2003. Numerical modelling of ice-jam flooding on the peace-Athabasca Delta. Hydrol. Process. 17 (18), 3685–3702.

Beltaos, S., 2010. Internal strength properties of river ice jams. Cold Reg. Sci. Technol. 62 (2010), 83–91.

Beltaos, S., 2011. Developing winter flow rating relationships using slope-area hydraulics. River Res. Appl. 27 (9), 1076–1089.

Beltaos, S., 2014. Comparing the impacts of regulation and climate on ice-jam flooding of

the peace-Athabasca Delta. Cold Reg. Sci. Technol. 108, 49–58.

Beltaos, S., Burrell, B.C., 2015. Hydroclimatic aspects of ice-jam flooding near Perth-Andover, New Brunswick. Can. J. Civ. Eng. 42 (9), 686–695.

Beltaos, S., Carter, T., 2009. Field studies of ice breakup and jamming in lower Peace River, Canada. Cold Regions Science and Technology Journal. 56 (2–3), 102–114.

Beltaos, S., Tang, P., 2013. Applying HEC-RAS to simulate river ice jams: snags and practical hints. In: Proc. 17th Workshop on River Ice, held at Edmonton, July 21-24, CGU HS Committee on River Ice Processes and the Environment, Edmonton, pp. 415–430.

Beltaos, S., Wong, J., 1986. Downstream transition of river ice jams. J. of Hyd. Eng. ASCE 112 (2), 91–110.

Beltaos, S., Prowse, T.D., Carter, T., 2006a. Ice regime of the lower Peace River and ice-jam flooding of the Peace-Athabasca Delta. Hydrol. Process. 20 (19), 4009–4029.

Beltaos, S., Prowse, T., Bonsal, B., MacKay, R., Romolo, L., Pietroniro, A., Toth, B., 2006b. Climatic effects on ice-jam flooding of the peace-Athabasca Delta. Hydrol. Process. 20 (19), 4031–4050.

Beltaos, S., Tang, P., Rowsell, R., 2012. Ice jam modelling and field data collection for flood forecasting in the Saint John River, Canada. Hydrol. Process. 26, 2535–2545.

Carey, K.L., 1966. Observed configuration and computed roughness of the underside of river ice, St. Crois River, Wisconsin. In: U.S. Geological Survey Prof. Paper 550-B, pp. B192–B198.

Carey, K.L., 1967. The underside of river ice, St. Crois River, Wisconsin. In: U.S. Geological Survey Prof. Paper 575-C, pp. B195–B199.

Carson, R., Beltaos, S., Groenevelt, J., Healy, D., She, Y., Malenchak, J., Morris, M., Saucet, J.-P., Kolerski, T., Shen, H.T., 2011. Comparative testing of numerical models of river ice jams. Can. J. Civ. Eng. 38, 669–678.

Chang, J., Wang, X., Li, Y., Wang, Y., 2016. Ice regime variation impacted by reservoir operation in the Ning-Meng reach of the Yellow River. Nat. Hazards 80, 1015–1030. https://doi.org/10.1007/s11069-015-2010-5.

Demuth, M.N., Hicks, F.E., Prowse, T.D., McKay, K., 1996. A numerical modelling analysis of ice jam flooding on the Peace/Slave River, Peace-Athabasca Delta. Peace-Athabasca Delta Technical Studies - P-ADJAM, Sub-component of Task F.2: Ice Studies. National Hydrology Research Institute Contribution Series CS-96016, Saskatoon, Canada, 33 pp. + figures, appendices. In: Peace-Athabasca Delta Technical Studies Appendices: I, Understanding the Ecosystem, Task Reports.

Flato, G.M., Gerard, R., 1986. Calculation of ice jam profiles. In: Proceedings, 4th Workshop on River Ice, Montreal, Canada, Paper C-3. CGU-HS Committee on River Ice Processes and the Environment, Edmonton, Canada.

Giroux, S., 1997a. 1996 Peace-Athabasca Delta Flood Report. Wood Buffalo National Park, Fort Chipewyan, Alberta, Canada.

Giroux, S., 1997b. 1997 Peace-Athabasca Delta Flood Report. Wood Buffalo National Park, Fort Chipewyan, Alberta, Canada.

HEC-RAS, 2010. Hydraulic Reference Manual, Version 4.1. US Army Corps of Engineers HEC, Davis, CA.

Henderson, F.M., 1966. Open Channel Flow. The Macmillan Co., New York, Toronto.

Hydro, B.C., 2013. Response to "impacts of the proposed site C dam on the hydrologic recharge of the peace-Athabasca Delta" (carver 2013). Submission to the Site C Joint Review Panel, December 18, 2013. http://www.acee.gc.ca/050/documents/p63919/97196E.pdf.

Jasek, M., 2017. Peace River 2014 break-up and ice jam at the peace-Athabasca Delta: field investigations and analysis. In: BC Hydro Generation Resource Management Engineering Report No. E1312.

Jasek, M., Pryse-Phillips, A., 2015. Influence of the proposed site C hydroelectric project on the ice regime of the Peace River. *Canadian Journal of Civil Engineering*, 2015 42 (9), 645–655.

Kellerhals, R., Neill, C.R., Bray, D.I., 1972. Hydraulic and geomorphic characteristics of rivers in Alberta. In: River Engineering and Surface Hydrology Report 72–1. Canada, Research Council of Alberta, Edmonton 52 p.

Nezhikhovskiy, R.A., 1964. Coefficients of roughness of bottom surface on slush-ice cover. In: Soviet Hydrology, Washington, Am. Geoph. Union, pp. 127–150.

Pariset, E., Hausser, R., Gagnon, A., 1966. Formation of ice covers and ice jams in rivers. Journal of the hydraulics division. ASCE Vol. 92 (HY6), 1–24.

Peters, D.L., Buttle, J.M., 2010. The effects of flow regulation and climatic variability on obstructed drainage and reverse flow contribution in a Northern River-Lake-Delta complex, Mackenzie Basin headwaters. River Res. Appl. 26, 1065–1089.

Peters, D.L., Prowse, T.D., Pietroniro, A., Leconte, R., 2006. Flood hydrology of the peace-Athabasca Delta, northern Canada. Hydrol. Process. 20, 4073–4096.

PFSRB (Partners FOR the Saskatchewan River Basin), 2009. From the Mountains to the Sea: The State of the Saskatchewan River Basin. Printed in Canada. http://www.saskriverbasin.ca/pages/state_of_the_basin_report.html (accessed 25.06.18).

Prowse, T.D., Conly, M., 1998. Impacts of climatic variability and flow regulation on ice jam flooding of a northern Delta. Hydrol. Process. 12, 1589–1610.

Prowse, T.D., Peters, D., Beltaos, S., Pietroniro, A., Romolo, L., Toyra, J., Leconte, R., 2002. Restoring ice-jam floodwater to a drying Delta ecosystem. Water Int. 27 (1), 58–69.

Serré, N., Liferov, P., Evers, K.-U., 2010. Experimental studies of ice ridge loads on structures. Proc. HYDRALAB III Joint User Meeting, Hannover 227–230. http://hydralab.eu/assets/history/Proceedings_Final_210110.pdf Feb. 2010.

Straka, J., Gray, Q., 2014. WBNP Flood Monitoring Report: Flood Extent, May 2014. Parks Canada, Fort Smith, NWT 17 p.

Tang, P., Beltaos, S., 2008. Modelling of river ice jams for flood forecasting in New Brunswick. In: Proceedings, 65th eastern snow conference (R. Hellström and S. Frankenstein, eds), Fairlee. Bridgewater State College and ERDC-CRREL, Vermont, USA, pp. 167–178.

Timoney, K.P., 2009. Three centuries of change in the peace–Athabasca Delta, Canada. Clim. Chang. 93, 485–515.

UNESCO, 2017. Reactive Monitoring Mission to Wood Buffalo National Park, Canada. In: Joint Mission report of World Heritage Centre and International Union for Conservation of Nature, Paris, March 2017, . http://whc.unesco.org/en/list/256/documents/.